SUPPLEMENTAL DATA

for "Dynamic distribution of muscle-specific calpain in mice has a key role in physical-stress adaptation and is impaired in muscular dystrophy" by Koichi Ojima *et al*.

Supplemental Table S1

DNA microarray analysis of skeletal muscle cells of WT and p94KI mice

Increase in p94KI

Fold change	*gene*	product name	aliases	probe Ac.No.
5.34	***Ddit4***	DNA-damage-inducible transcript 4	REDD1, RTP801, Dig2, FLJ20500, DKFZp564O2071	AI849939
3.25	***AA675344***	-	-	AA675344
3.06	***Prom1***	prominin-1	AC133, CD133, MSTP061, PROML1,	AF039663
2.18	***Slc30a1***	solute carrier family 30 (Zn transporter), member 1	ZNT1, ZnT-1	U17132
2.04	***Hspca***	heat shock 90 kDa protein 1, α	HSPC1, Hsp89, Hsp90, FLJ31884, LAP2, HSP86, HSP90A	J04633
2.02	***Kcna5***	potassium voltage-gated channel, shaker-related subfamily, member 5	HK2, HPCN1, KV1.5, PCN1, Kv1.5	L22218
1.89	***Mig-6***	mitogen-inducible gene 6 protein	GENE-33, MIG6, RALT(receptor-associated late transducer)	AI853531
1.78	***Gucy1b3***	guanylate cyclase 1, soluble, β1	guanylate cyclase 1 soluble β3, GUCB3, GC-SB3, GUC1B3, GUCSB3, GC-S-β-1	AF020339
1.70	***Mtss1l***	metastasis suppressor 1-like	insulin receptor tyrosine kinase substrate p53 (IRSp53)-related protein (ABBA-1)	AI846678
1.67	***Prkca***	PKCα	PKCA	M25811
1.64	***Angpt1***	angiopoietin 1	KIAA0003, ANG-1	U83509
1.64	***Rabep1***	rabaptin, RAB GTPase binding effector protein 1	neurocrescin, RAB5EP, RABPT5, rabaptin-5, rabaptin-5α, rabaptin-4, RABPT5A	D86066
1.63	***Mki67ip***	MKI67 (FHA domain) interacting nucleolar phosphoprotein	Nopp34, NIFK	AI852665
1.60	***Tyms-ps***	thymidylate synthase, pseudogene	-	M30774
1.56	***Cma1***	chymase 1, mast cell	mast cell protease I, CYH, CYM, MCT1, chymase, heart	M68898
1.52	***Lrrc23***	leucine rich repeat containing 23	Lrpb7	AV257486
1.50	***Sox17***	SRY (sex determining region Y)-box 17	transcription factor SOX-17	D49473

1.50	***Dnajb2***	DnaJ (Hsp40) homologue, subfamily B, member 2	HSJ1, HSPF3, HSJ-1, DnaJ protein homolog 1, heat shock 40 kDa protein 3	AI843164
1.50	***Pnpla2***	patatin-like phospholipase domain containing 2	TTS-2.2, 1110001C14Rik, transport-secretion protein 2.2	AW121217

Decrease in p94KI

fold	***gene***	**product name**	**aliases**	**probe Ac.No.**
4.46	***Itgb2***	Integrin β2	CD18, MFI7, LFA-1/CR3/p150,95 β-subunit, Complement receptor C3 β-subunit	M31039
2.87	***Alas2***	δ-aminolevulinaste, synthase 2 (sideroblastic/hypochromic anemia)	ASB, ANH1, XLSA, hereditary iron-loading anemia	M15268
2.75	***1500010J02Rik***	hypothetical protein FLJ22170		AW124900
2.48	***Idh3a***	isocitrate dehydrogenase 3 (NAD^+) alpha	isocitric dehydrogenase, EC 1.1.1.41	AV095915
2.31	***Cadps***	Ca^{2+}-dependent secretion activator	CAPS, KIAA1121, CAPS1	D86214
2.30	***Hba1***	hemoglobin, α1	CD31, HBA2	V00714
1.68	***Hba2***	hemoglobin, α2		AV003378
2.26	***Fap***	α fibroblast activation protein	DPPIV, FAPA, SEPRASE, integral membrane serine proteinase, 170-kDa melanoma membrane-bound gelatinase	Y10007
2.12	***Znf281***	zinc finger protein 281	ZBP-99, ZNP-99, GC-box-binding zinc finger protein 1, GZP1, ZBP99	AI850113
2.03	***Scd***	stearoyl-CoA desaturase (δ-9-desaturase)	FADS5, PRO0998, fatty acid desaturase, acyl-CoA desaturase	AV327760
1.93	***Evi2a***	ectropic viral integration site 2A	EVI2, EVDA	M34896
1.91	***Tle4***	transducin-like enhancer of split 4 (E(sp1) homologue, drosophila)	E(spl), ESG, KIAA1261, Groucho4	U61363
1.77	***AI506816***	(BC028259, viral LTR?)	-	C78850
1.75, 1.65	***Rbbp6***	retinoblastoma binding protein 6	MY038, RBQ-1, DKFZp761B2423	AI661370, AV330213
1.71	***Cd200***	CD200 antigen	MOX1, MOX2, antigen identified by monoclonal antibody MRC OX-2, MRC, OX-2, OX-2 membrane glycoprotein, My033	AF029215
1.69	***Dsp***	desmoplakin	DPI, DPII, KPPS2, PPKS2, DP, 250/210 kDa paraneoplastic pemphigus antigen	AA600542
1.67	***Clns1a***	chloride channel, nucleotide-sensitive, 1A	DLCI, ICln, CLNS1B, methylosome subunit pICln, chloride conductance regulatory protein ICln, chloride ion current inducer protein ClCI, reticulocyte pICln	U53455

1.67	***Tp53bp1***	tumor protein p53 binding protein, 1	p202, 53BP1	AW048394
1.65	***Ppp2r5c***	protein phosphatase 2, regulatory subunit B (B56), γ isoform	PP2A, B subunit, B' γ, B56 γ, PR61 γ, R5 γ isoform, KIAA0044	U59418
1.64	***Igfbp5***	insulin-like growth factor binding protein 5	IGFBP-5, IBP-5, IGF-binding protein 5, IBP5	L12447
1.63	***Ermp1***	endoplasmic reticulum metallopeptidase 1	FLJ23309, KIAA1815	AI851365
1.62	***Crip1***	cysteine-rich protein 1 (intestinal)	CRIP cysteine-rich intestinal protein, CHIP cysteine-rich heart protein, hCRHP	M13018
1.61	***Mrc1***	mannose receptor, C type 1	CD206, MMR, macrophage mannose receptor precursor	Z11974
1.61	***Chp***	Ca^{2+}-binding protein P22	SLC9A1BP, Sid470, calcineurin B homologue	AB025217
1.60	***Cnn2***	calponin 2	calponin H2, smooth muscle, neutral calponin	Z19543
1.57	***Alg2***	asparagine-linked glycosylation 2 homologue (yeast, α-1,3-mannosyltransferase)	CDGli, FLJ14511, hALPG2, GDP-Man:Man(1)GlcNac(2)-PP-dolichol mannosyltransferase	AI834815
1.54	***Cdan1***	congenital dyserythropoietic anemia, type 1	CDA-I, CDAI, codanin, UNQ664/PRO1295	AA691078
1.53	***Slc11a2***	solute carrier family 11 (proton-coupled divalent metal ion transporters), member 2	NRAMP2, DCT1, DMT1, OK/SW-cl.20, natural resistance-associated macrophage protein 2	L33415
1.53	***Staf42***	SPT3-associated factor 42	RP1-9E21.4	AW125318
1.53	***Ints7***	integrator complex subunit 7		AW120890
1.53	***Prss23***	protease, serine, 23	SPUVE, SIG13, UNQ270/PRO307, putative secreted protein ZSIG13	AW228316
1.52	***Siat8d***	sialyltransferase 8D (α-2,8-polysialyltransferase)	PST, PST1, ST8Sia IV, CMP-N-acetylneuraminate-poly-α-2,8-sialyl transferase, polysialyltransferase-1	X86000
1.52	***Fbxo3***	F-box protein 3	1200002G09Rik, 1700026K02Rik, Fba	AW046579
1.50	***Cpxm2***	carboxypeptidase X (M14 family), member 2	4632435C11Rik, UNQ676/PRO1310, potential carboxypeptidase-like protein X2	AF017639
1.50	***Rpa3***	replication protein A3, 14 kDa	replication protein A 14 kDa subunit, RP-A, RF-A	AI848299

Gene expression profiles of skeletal muscle from two independent WT and p94KI mice (total of four) were compared using an Affymetrix U74A DNA chip as described previously (1), and genes that showed significantly different expression between WT and p94KI are listed. Note that none of the products of these genes are included in Supplemental Figure S10.

Supplemental Table S2

Abs used in this study

Antigen name	Dilution (Blot)	Dilution (Histology)	Company/Reference
p94:IS2C	1:3000	-	(2)
p94:pNS	-	1:300	(3)
connectin/titin N2A	-	1:500	(4)
MARP2/ANKRD2	1:2000	1:500	(5)
	1:1000	1:500	Protein Tech Group, Inc.
laminin α2	-	1:300	Alexis Biochemicals
sarcomeric-α-actinin	-	1:1000	Sigma
His-tag	1:1000	-	Novagen
M-cadherin	-	1:500	Santa Cruz Biotechnology, Inc., clone#12G4
Dysferlin	-	1:40	Novocastra laboratories Ltd

-: not used in this study

Supplemental Table S3

PCR primers used in this study

Name/use	Direction	Sequence
lox1s	sense	5'-cgc gga tcc ata tga taa ctt cgt ata gca tac att ata cga agt tat tcg agc agt gtg gtt ttg ca-3'
lox1a	antisense	5’-cgc gga tcc ata tga taa ctt cgt ata gca tac att ata cga agt tat gat ccg aac aaa cga ccc aa-3’
lox2s-1	sense	5'- cat aca tta tac gaa gtt atc gat gag ctc gag cag tgt ggt t-3'
lox2s-2	sense	5'-cgc gga tcc ata tga taa ctt cgt ata gca tac att ata cga a-3'
lox2a	antisense	5’-atc ctg atc gac aag acc-3’
5’ probe	sense	5'-ctg caa gaa cat ggt gct ta-3'
	antisense	5'-gag acg ctt cct tgt gcg-3'
3’ probe	sense	5'-tgg gga ccg tca tga caa tgc-3'
	antisense	5'-tct ggg ggc gct agt cag tct c-3'
ex.3 probe	sense	5'-tcc cga gtc att agc tat gg-3'
	antisense	5'-cca cac gtg gat gta agt tg-3'
PCR1	sense	5’-aga ccc atc tgt cct tgt tg-3’
	antisense	5’-aaa ggc agt ctg gag tct ag-3’
PCR2	sense	5'-tcc cga gtc att agc tat gg-3'
	antisense	5'-cca cac gtg gat gta agt tg-3'

REFERENCES for SUPPLEMENTAL DATA

1. Witt, C.C., Ono, Y., Puschmann, E., McNabb, M., Wu, Y., Gotthardt, M., Witt, S.H., Haak, M., Labeit, D., Gregorio, C.C., et al. Induction and myofibrillar targeting of *CARP*, and suppression of the Nkx2.5 pathway in the MDM mouse with impaired titin-based signaling. *J. Mol. Biol.* 2004;336(1):145-154.
2. Ojima, K., Ono, Y., Doi, N., Yoshioka, K., Kawabata, Y., Labeit, S., and Sorimachi, H. Myogenic stage, sarcomere length, and protease activity modulate localization of muscle-specific calpain. *J. Biol. Chem.* 2007;282(19):14493-14504.
3. Sorimachi, H., Toyama-Sorimachi, N., Saido, T.C., Kawasaki, H., Sugita, H., Miyasaka, M., Arahata, K., Ishiura, S., and Suzuki, K. Muscle-specific calpain, p94, is degraded by autolysis immediately after translation, resulting in disappearance from muscle. *J. Biol. Chem.* 1993;268(14):10593-10605.
4. Trombitas, K., Greaser, M., Labeit, S., Jin, J.P., Kellermayer, M., Helmes, M., and Granzier, H. Titin extensibility in situ: entropic elasticity of permanently folded and permanently unfolded molecular segments. *J. Cell Biol.* 1998;140(4):853-859.
5. Hayashi, C., Ono, Y., Doi, N., Kitamura, F., Tagami, M., Mineki, R., Arai, T., Taguchi, H., Yanagida, M., Hirner, S., et al. Multiple molecular interactions implicate the connectin/titin N2A region as a modulating scaffold for p94/calpain 3 activity in skeletal muscle. *J. Biol. Chem.* 2008;283(21):14801-14814.
6. Thompson, S., Clarke, A.R., Pow, A.M., Hooper, M.L., and Melton, D.W. Germ line transmission and expression of a corrected *HPRT* gene produced by gene targeting in embryonic stem cells. *Cell* 1989;56(2):313-321.
7. Lakso, M., Pichel, J.G., Gorman, J.R., Sauer, B., Okamoto, Y., Lee, E., Alt, F.W., and Westphal, H. Efficient in vivo manipulation of mouse genomic sequences at the zygote stage. *Proc. Natl. Acad. Sci. USA* 1996;93(12):5860-5865.

Supplemental Figure S1. Generation of p94KI mice.

(**A**) Targeting scheme for the p94KI construct. A missense mutation [6th T to A in exon 3 of the p94/calpain 3 gene, *Capn3* (agGGGAC***T***GCTGGTTT -> agGGGAC***A***GCTGGTTT)], was introduced into exon 3 by performing PCR on a 1.7-kb *Bst*PI fragment subcloned from 129S mouse genomic DNA. The missense mutation changed Cys129, an amino acid residue in the catalytic center of p94, to Ser, and created a *Pvu*II site. The complete nucleotide sequence of the mutated 1.7-kb *Bst*PI fragment was verified by DNA sequencing.

A neomycin-resistance gene (*neoR*) flanked by loxP sequences was constructed as follows. A DNA fragment was generated by PCR using primers lox1s and lox1a (see Table S3) and pMC1neo polyA$^+$ vector DNA (Stratagene) as a template. The 3'-part of the fragment was rescued by cutting it with *Rsr*II and *Bam*HI, which resulted in a *neoR*-loxP 3' fragment of 255 bp, and the fragment was cloned into the 3.6-kb pMC1neo polyA$^+$/*Rsr*II-*Bam*HI fragment (Plasmid A). The 5'- loxP part was amplified by performing half-nested PCR, first with primers lox2s-1 and lox2a and then with lox2s-2 and lox2a, on pMC1neo polyA$^+$ plasmid DNA. The amplified PCR fragment was cloned into the TA TOPO cloning vector (Invitrogen), and the 5'-loxP-containing *Spe*I-*Cla*I fragment (*Spe*I-TOPO vector-*Nde*I-loxP-*Cla*I) was used for ligation with the *Xho*I-*Spe*I fragment (*Xho*I-*neoR*-loxP-*Nde*I-*Spe*I) of Plasmid A described above, resulting in loxP-*neoR*-loxP flanked by *Nde*I sites (*Nde*I-loxP-*neoR*-loxP-*Nde*I) in the TOPO vector. The *neoR* cassette was cut by *Nde*I and inserted into the *Nde*I site located 280-bp downstream of the exon 3-intron 3 junction of *Capn3*.

The C129S mutation and *neoR* cassette insertion were then ligated together, and the *Hind*III-*Bgl*II fragment of pMCDT-A(A+T/pau) (Oriental Yeast) was added to the 3'-end of the final targeting vector. The targeting vector was introduced into mouse E14tg2a modified ES cells (6) by electro-transfection (*Capn3*$^{C129S\text{-}neo}$). Among the 120 ES colonies that survived in G418 selection medium, 6 were positive for the targeting vector as determined by PCR screening (see B). The

recombinant ES cell lines were also characterized by Southern blot analysis (see C). Isolated genomic DNA was digested with *Afl*II or *Stu*I+*Bam*HI, and hybridized with the 5' or 3' probe indicated. Cell lines #32 and #55 were used for blastocyst injection, and both produced germline-transmitted chimeric mice. The F1 heterozygotes (*Capn3*$^{C129S\text{-}neo/+}$) were analyzed by Southern blot analysis (see D) to confirm proper recombination, and were crossed with Tg mice expressing the Cre recombinase in germline cells, B6.FVB-TgN(EIIa-Cre)C5379Lmgd (7). Both the #32 and #55 lines produced mice with the C129S mutation without *neoR* (*Capn3*^{C129S}), which was confirmed by PCR and Southern blot analyses (see D), and eventually showed apparently identical phenotypes (data not shown). Therefore, the #55 line was used for further experiments. The p94KI mice were backcrossed with C57BL/6 J mice for more than 8 generations. The mouse genotypes were determined by genomic Southern blot and PCR analyses. The PCR primers are listed in Table S3.

The numbers indicate exons. LoxP sites were inserted on both sides of a *neoR* cassette. PCR1 and PCR2 indicate the amplified regions used to detect the allele by homologous recombination. DT-A, diphtheria toxin A fragment.

(**B**) PCR screening of ES cell colonies. Genomic DNA isolated from G418-resistant ES cell lines was subjected to PCR amplification of the targeted region shown in (A) as "PCR1". Closed and open arrowheads indicate the amplified bands of the WT and mutant samples, respectively. ht, heterozygous; HM, homozygous.

(**C**) Southern blot analysis of F1 mice. Genomic DNA isolated from the tails of mice resulting from crosses between targeted chimeras and WT mice was digested with *Afl*II or *Stu*I+*Bam*HI, and subjected to Southern blot analysis using the 5' and 3' probes indicated in A. Closed and open arrowheads indicate bands corresponding to the WT and mutant alleles, respectively. ht, heterozygous.

(**D**) Southern blot and PCR analysis of p94KI. Genomic DNA from mice derived from crosses between p94KI and WT mice was digested with *Pvu*II and subjected to Southern blot analysis using the ex.3 probe indicated in A (upper). The same genomic DNA was subjected to PCR amplification using the same conditions as in (B) (lower). Closed and open arrowheads indicate bands corresponding to the WT and mutant alleles, respectively. ht, heterozygous; HM, homozygous.

(**E**) Confirmation of the C129S mutation in p94KI mice. Genomic DNA from the mouse tail was amplified by PCR and digested by *Pvu*II, generating fragments of 662 and 108 bp (open arrowheads) for homozygotes (HM), 730 bp (closed arrowheads) for WT mice (WT), and 108, 662, 730, and 770 bp for heterozygotes (ht).

(**F**) Proteolytic inactivity of p94 in p94KI mice. Equal amounts of protein from skeletal muscle lysates of WT and p94KI mice (15-wk old) were incubated with 10 mM EDTA or 5 mM $CaCl_2$ at 30°C for 30 min. Full-length p94 (arrow) and its proteolytic fragments (arrowheads) were detected with an anti-p94 (pIS2C) Ab. -, no treatment; E, +EDTA; C, +Ca^{2+}.

Supplemental Figure S2. Exercise-induced autolysis and localization change of p94.

Full-length p94 and its fragments in WT, WT-ex, p94KI, and p94KI-ex mice were analyzed by immunoblotting using an anti-p94 (pIS2C) Ab in the Ppt (A), total (D), and Sup (see Figure 2A) fractions of TA muscle (representative blots are shown). In WT-ex and p94KI-ex mice, the TA muscles were isolated immediately after exercise. Full-length p94 (C, F, G) and one of its proteolytic fragments (B, E, and Figure 2B) indicated in A and D as closed and open arrowheads, respectively, were quantified by normalizing to CBB-stained Mhc (Ppt and total) or actin (Sup). cont, COS-expressed human p94:C129S; *, $P<0.01$ (vs WT).

Supplemental Figure S3. Frequency distribution of EBD-negative and -positive myofiber CSAs in the Gastrocnemius (GC) of p94KI-ex mice on post-exercise day 1.

A total of 378 EBD-negative (undamaged) and 110 EBD-positive fiber profiles were traced in two sections from each of three p94KI-ex mice. The average CSAr was 1,817 μm^2 and 1,933 μm^2 for the EBD-negative and -positive myofibers, respectively, showing no statistically significant difference.

Supplemental Figure S4. Normal muscle regeneration was observed in exercised p94KI mice.

Muscle regeneration processes were observed in H&E-stained gastrocnemius muscles from WT-ex (A-C) and p94KI-ex (D-F) mice. Muscles were prepared on the indicated days after exercise. The invading cells and proliferating myogenic cells were observed in p94KI-ex mice (dotted areas in D and E). Small-diameter myofibers with central nuclei are de novo regenerated myofibers (F). WT-ex mice showed no obvious damage (A-C). Bars, 100 μm.

Supplemental Figure S5. **Control experiments for the FRAP experiments in Figure 3C.**

(A and B) FRAP observation of GFP expressed in cultured myotubes. Representative series of micrographs are shown. GFP was exogenously expressed in cultured myotubes from WT (A) or p94KI (B) mice by the transfection of pEGFP empty vector into the myotubes. GFP showed diffuse and uniform signals in the cytosol without striation. Reference images were acquired before photobleaching (Pre). Rectangles indicate the photobleached areas. (**C**) Relative fluorescence intensities in the areas were calculated by LSM software as the ratio of GFP intensity at each time point to that before photobleaching, and plotted against time. The GFP signal could not be photobleached to 0% because the mobility of GFP in the cytosol was too fast, and was quickly recovered to almost 90% within 30 s.

Supplemental Figure S6. Statistical tests for the significant difference between the k values for

p94WT and p94:C129S in Figure 3C.

(A) Scatter plots of $\boldsymbol{R}$ *vs.* time and analysis of covariance. Observation time ($\boldsymbol{t}$, s) and relative recovery of GFP fluorescence intensity ($\boldsymbol{R}_{\mathrm{WT}}$ and $\boldsymbol{R}_{\mathrm{CS}}$ for p94WT (WT) and p94:C129S (CS) experiments, respectively) were well fitted to the equation, $\boldsymbol{R} = M(1 - e^{-k\boldsymbol{t}})$, and we obtained estimated values of M and k for both WT and CS (M_{WT}, k_{WT}, M_{CS}, and k_{CS} are estimated to be 0.590, 0.0104, 0.619, and 0.00538, respectively, as shown here and in Figure 3C). First, the following two hypotheses are taken: H_0: $k_{\mathrm{WT}} = k_{\mathrm{CS}}$ and H_1: $k_{\mathrm{WT}} \neq k_{\mathrm{CS}}$ (both sides)

Under H_1, the residual sums of squares for WT and CS are calculated using each of 400 data pairs (($\boldsymbol{R}_{\mathrm{WT}i}$, $\boldsymbol{t}_i$) and ($\boldsymbol{R}_{\mathrm{CS}i}$, $\boldsymbol{t}_i$) [i = 1 to 400]):

$\Delta\mathrm{WT} = \sum_{i=1}^{400}\left(\boldsymbol{R}_{WT_i} - M_{WT}(1 - e^{-k_{WT}\boldsymbol{t}_i})\right)^2 = 0.562$; $\Delta\mathrm{CS} = \sum_{i=1}^{400}\left(\boldsymbol{R}_{CS_i} - M_{CS}(1 - e^{-k_{CS}\boldsymbol{t}_i})\right)^2 = 1.590$; $\Delta 1 = \Delta\mathrm{WT} + \Delta\mathrm{CS} = 2.152$

Under H_0, all 800 data pairs (400 WT and 400 CS) were fitted as described above, and the following equation was obtained:

$\boldsymbol{R}_{\mathrm{T}} = M_{\mathrm{T}}(1 - e^{-k_{\mathrm{T}}\boldsymbol{t}})$, where M_{T}, and k_{T} are estimated to be 0.5859 and 0.00788 by the least squares method.

The residual sums of squares for all 800 data pairs were calculated using two of the 400 data pairs (($\boldsymbol{R}_{\mathrm{WT}i}$, $\boldsymbol{t}_i$) and ($\boldsymbol{R}_{\mathrm{CS}i}$, $\boldsymbol{t}_i$) [i = 1 to 400]):

$\Delta 2 = \sum_{i=1}^{400}\left(\boldsymbol{R}_{WT_i} - M_T(1 - e^{-k_T\boldsymbol{t}_i})\right)^2 + \sum_{i=1}^{400}\left(\boldsymbol{R}_{CS_i} - M_T(1 - e^{-k_T\boldsymbol{t}_i})\right)^2 = 3.834$

A statistical value, F is defined as follows: $F = \frac{\Delta 2 - \Delta 1}{\Delta 1/(N-4)} = (\frac{\Delta 2}{\Delta 1} - 1) \times (N - 4) = 578.7$, where N = the number of total samples (in our case, 400 + 400 - 56 (inappropriate data) = 744). By analysis of covariance, under H_0, F is known to follow the F distribution with the degrees of freedom, ν_1 =1 and $\nu_2 = N$-4 [$F_{1,\,N\text{-}4}$]. Since the upper point where $F_{1,\,N\text{-}4}$ shows 0.001 probability ($F_{1,\,N\text{-}4}(\alpha = 0.001)$) is 10.91, and is less than the calculated F, and thus, H_0 is rejected with a significance level

of 0.001 (P value for acceptance of H_0 is 1.48 x 10^{-96}). Therefore, it is concluded that $k_{WT} \neq k_{CS}$.

(B) Distribution of K and non-parametric tests. Using estimated M_{WT} and M_{CS}, k_{WT} and k_{CS} can be calculated for each of 400 data pairs of $\boldsymbol{R}$ and $\boldsymbol{t}$ for each of WT and CS. These two sets of k values, K_{WT} and K_{CS}, have 400 elements each, the distributions of which are shown here. Non-parametric tests for the difference between K_{WT} and K_{CS} were performed using Origin™ 8 Pro software (Origin Lab Corp) and an "R" package "lawstat". For the Kolmogorov-Smirnov test and Wilcoxon-Mann-Whitney test, let H_0: median (K_{WT}) = median (K_{CS}) and H_1: median (K_{WT}) > median (K_{CS}). The Kolmogorov-Smirnov test showed a D value of 0.26 and P value of 2.5 x 10^{-12}, and the Wilcoxon-Mann-Whitney test showed a U value of 63,358 and P value of 3.5 x 10^{-7} (Origin™ 8 Pro). Therefore, both tests indicated that the medians of K_{WT} and K_{CS} were significantly different with a risk rate of 0.001.

For the Brunner-Munzel test, let H_0: $P = 0.5$ and H_1: $P > 0.5$, where $P = P(K_{WT} > K_{CS}) + \frac{1}{2} P(K_{WT} = K_{CS})$. This test does not assume any distribution pattern or homoscedasticity. Calculation with an "R" package "lawstat" showed a degree of freedom of 737.929, W value of 45.763, estimated P value of 0.927, and P value of less than 2.2 x 10^{-16}. Therefore, the Brunner-Munzel test also indicated that the averages of K_{WT} and K_{CS} were significantly different with a risk rate of 0.001. All of these analyses indicated that k_{WT} and k_{CS} estimated by two data sets, K_{WT} and K_{CS}, were significantly different, i.e., that WT and CS have significantly different recovery rates.

All four statistical tests described above also showed significant difference between the estimated WT and p94KI (KI) curves ($\boldsymbol{r} = Ae^{-\boldsymbol{kl}}$; $A_{WT} = 4.56$, $k_{WT} = 1.01$, $A_{KI} = 8.80$, $k_{KI} = 1.18$) shown in Figure 3Q (Parameters, in order, are: $N = 377$, $F_{1, N-4}(\alpha = 0.001) = 11.0$, $F = 39.9$, $P = 7.76$ x 10^{-10}; $D = 0.68$ (for A) and 0.54 (for k), $P = 6.46$ x 10^{-39} and 1.69 x 10^{-24}; $U = 3{,}020$ and 5,527, $P = 3.73$ x 10^{-44} and 5.98 x 10^{-31}; $df = 368$ and 365, $W = 29.6$ and 17.7, $p = 0.915$ and 0.845, $P < 2.2$ x 10^{-16} and < 2.2 x 10^{-16}).

Supplemental Figure S7. Change in the MARP2 level in WT and p94KI mice after exercise.

The MAPR2 protein amount in WT, WT-ex, p94KI, and p94KI-ex mouse muscles was analyzed by western blotting using an anti-MARP2 Ab. TA muscles (total extract) were isolated immediately after exercise. The Mhc bands stained by CBB, used as loading controls, are shown. Hairlines indicate lanes that were run on the same gel but were noncontiguous.

Supplemental Figure S8. Specificities of the anti-MARP2 Abs used in this study.

(**A**) Characterization of two anti-MARP2 Abs used in this study by immunoblot analysis. The anti-MARP2 Ab described in reference (5) and that purchased from Protein Tech Group Inc. are called "anti-MARP2" and "anti-Ankrd2" Abs for descriptive purposes here. To verify the specificity of these anti-MARP2 Abs, they were compared with those absorbed with an excess amount of recombinant His-tagged full-length human MARP2 protein (5). Sup fractions from WT (WT) and p94KI (p94KI) mouse TA muscles, and His-tagged full-length human MARP2 (His-MARP2, 50 ng/lane) as a positive control were used for immunoblot analyses with the indicated Abs. CBB-stained His-MARP2 and actin bands, used as a loading control, are shown.

(**B-S**) Characterization of the anti-MARP2 Ab by immunostaining. Muscle cross (B-M, T-e) and longitudinal (N-S, f-k) sections from WT (B-D, H-J, N-P, T-V, Z-b, f-h), and p94KI (E-G, K-M, Q-S, W-Y, c-e, i-k) mice were stained with anti-laminin α2 (B, E, H, K, T, W, Z, c), anti-MARP2 (C, F, O, R), absorbed anti-MARP2 (I, L), anti-Ankrd2 (U, X, g, j), absorbed anti-Ankrd2 (a, d), and anti-sarcomeric α-actinin (N, Q, f, i) Abs.

Nuclei were visualized with DAPI (light blue in B, D, E, G, H, J, K, M, P, S, T, V, W, Y, Z, b, c, e, h, k). Merged images are shown in D, G, J, M, P, S, V, Y, b, e, h, and k. Bars, 50 μm**.**

Supplemental Figure S9. MARP2 is expressed in the cytosol and in myonuclei, but not in the nuclei of satellite cells.

(**A-F**) To determine the localization of satellite cells, cryostat sections of TA muscles of WT (A-C) and p94KI (D-F) mice were immunostained with anti-M-cadherin (A and D) and anti-laminin α2 (B and E) Abs after blocking with MOM™ mouse Ig blocking reagent (Vector Laboratories, Inc.). Images were visualized by confocal fluorescence microscopy (LSM510, Zeiss). M-cadherin is a marker for satellite cells, which were located beneath the laminin-positive basement membrane (arrowheads in A, C, D, and F).

(**G-L**) Confocal micrographs of M-cadherin (G and J) and MARP2 (H and K) in muscles from exercised WT (G-I) and p94KI (J-L) mice. The nuclei of satellite cells had no MARP2 signals (arrowheads in G-L).

Merged images are shown at the right (C, F, I, and L). Insets in C, F, I, and L are magnified images of the regions marked by squares. Bars, 10 μm.

Supplemental Figure S10. Proteins with significantly different expression in the cytosol of WT and p94KI skeletal muscles.

Relative protein expression amounts of WT, WT-ex, p94KI, and p94KI-ex mice were analyzed by iTRAQ™-labeling, 2D-LC-MALDI-TOF/TOF, and ProteinPilot™ software. Proteins that have %Cov of non zero value and show p94KI/WT of WT/p94KI>1.1 are listed here in order of the p94KI/WT value (%Cov means % of amino acid residues (aar) included in the identified peptides with a confidence level of more than 95 against total aar of the protein). Ratios of greater than 1.1, greater than 1.2, less than 1/1.1 (0.91), and less than 1/1.2 (0.83) are marked by red, orange, pale blue, and blue colors, respectively. *P*-values were calculated by the ProteinPilot™ program for proteins that are identified by more than one peptide; otherwise, they are shown by "-". *P*-values

less than 0.05 are colored yellow. For proteins that had no *P*-value due to single MS/MS identification or a *P*-value of more than 0.05, MS/MS spectra were manually examined and verified, and are listed only if the MS/MS spectra were clear enough to represent a change in ratios. mRNA expression profiles are shown for genes on the DNA microarray (see Supplemental Table S1); NC, not significantly changed; -, not included in the microarray chip used.

Note that hexokinase 2, one of the rate-limiting enzymes for glycolysis, and factors involved in protein translation (EF-Tu and eEF-1γ), and proteasome subunits (PSMA4 and PSMD7) were upregulated in p94KI and WT-ex compared with WT (category **b** in Table 1). Members of this group may contribute to turnover of muscle cells by providing ATP, and producing and destructing proteins. Also, UbcH7, Nedd8, RSK-1 and S36mt, which are involved in protein degradation and translation systems, are also upregulated in WT-ex and p94KI (compared with WT) and p94KI-ex (compared with p94KI) (category **a** in Table 1). On the other hand, calsequestrin 1 (CASQ1), parvalbumin and myosin regulatory light chain 2, which binds Ca^{2+}, are all downregulated in p94KI and WT-ex compared with WT (category **d** in Table 1).

Troponin I2 (TNNI2) and nicotinamide phosphoribosyltransferase (NAMPT) were upregulated in p94KI (compared with WT), but downregulated in p94KI-ex (compared with p94KI), whereas WT-ex showed no difference from WT. Conversely, programmed cell death protein 11 (PDCD11 or ALG-4) and carbonic anhydrase 3 (CAR3) were downregulated in p94KI (compared with WT), but upregulated in p94KI-ex (compared with p94KI), whereas WT-ex showed no difference from WT. These proteins may correspond to those perturbed upon exercise without p94 protease activity, but are modulated to be unchanged during exercise in WT mice.

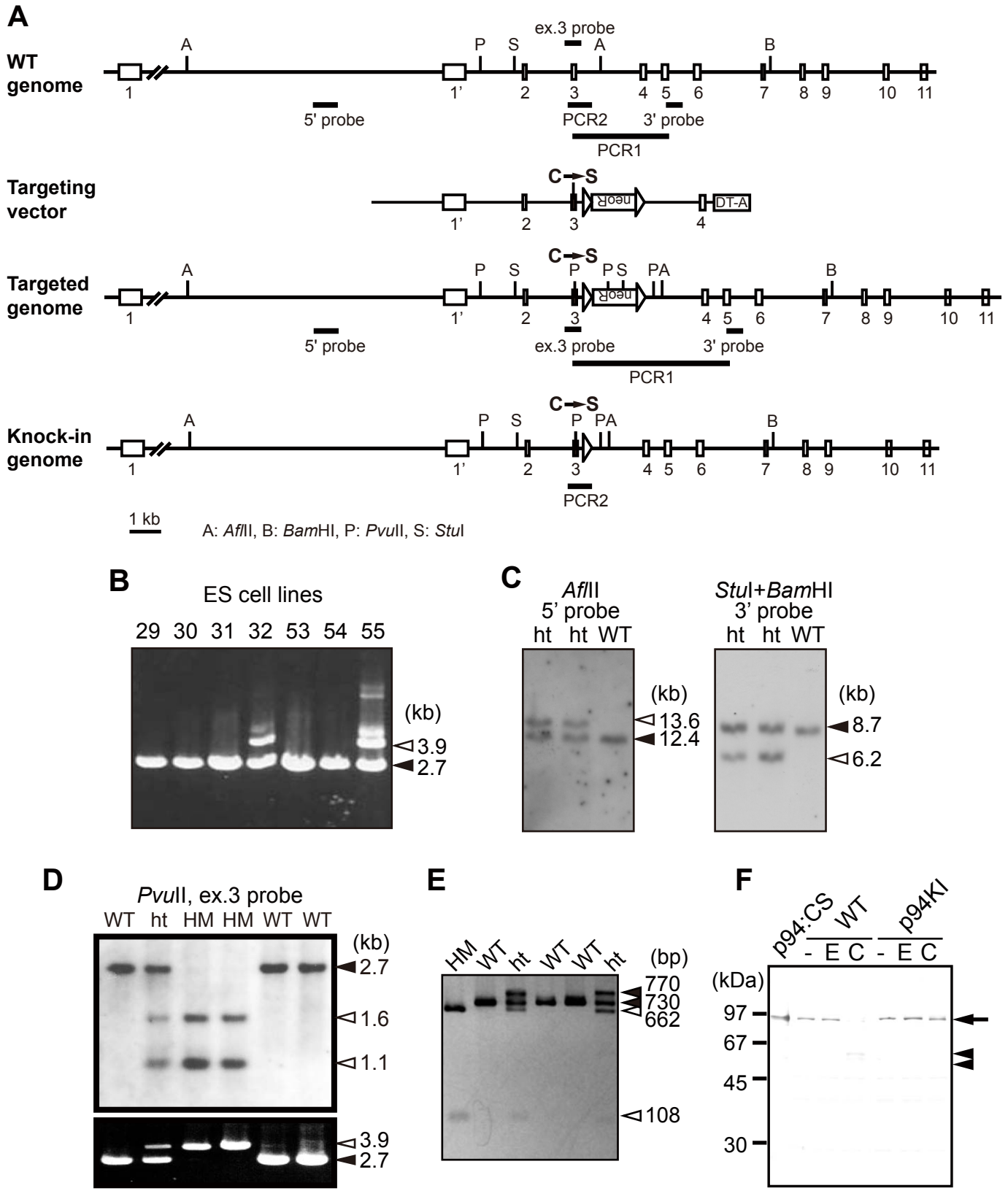

Supplemental Figure S1. Generation of p94KI mice.

(**A**) Targeting scheme for the p94KI construct. A missense mutation [6th T to A in exon 3 of the p94/calpain 3 gene, *Capn3* (agGGGACTGCTGGTTT -> agGGGACAGCTGGTTT)], was introduced into exon 3 by performing PCR on a 1.7-kb BstPI fragment subcloned from 129S mouse genomic DNA. The missense mutation changed Cys129, an amino acid residue in the catalytic center of p94, to Ser, and created a PvuII site. The complete nucleotide sequence of the mutated 1.7-kb BstPI fragment was verified by DNA sequencing. (*Legend cotinues on the next page.*)

(*Continued from the previous page*) A neomycin-resistance gene (*neoR*) flanked by loxP sequences was constructed as follows. A DNA fragment was generated by PCR using primers lox1s and lox1a (see Table S2) and pMC1neo polyA$^+$ vector DNA (Stratagene) as a template. The 3'-part of the fragment was rescued by cutting it with *Rsr*II and *Bam*HI, which resulted in a *neoR*-loxP 3' fragment of 255 bp, and the fragment was cloned into the 3.6-kb pMC1neo polyA$^+$/*Rsr*II-*Bam*HI fragment (Plasmid A). The 5'- loxP part was amplified by performing half-nested PCR, first with primers lox2s-1 and lox2a and then with lox2s-2 and lox2a, on pMC1neo polyA$^+$ plasmid DNA. The amplified PCR fragment was cloned into the TA TOPO cloning vector (Invitrogen), and the 5'-loxP-containing *Spe*I-*Cla*I fragment (*Spe*I-TOPO vector-*Nde*I-loxP-*Cla*I) was used for ligation with the *Xho*I-*Spe*I fragment (*Xho*I-*neoR*-loxP-*Nde*I-*Spe*I) of Plasmid A described above, resulting in loxP-*neoR*-loxP flanked by *Nde*I sites (*Nde*I-loxP-*neoR*-loxP-*Nde*I) in the TOPO vector. The *neoR* cassette was cut by *Nde*I and inserted into the *Nde*I site located 280-bp downstream of the exon 3-intron 3 junction of *Capn3*.

The C129S mutation and *neoR* cassette insertion were then ligated together, and the *Hind*III-*Bgl*II fragment of pMCDT-A(A+T/pau) (Oriental Yeast) was added to the 3'-end of the final targeting vector. The targeting vector was introduced into mouse E14tg2a modified embryonic stem (ES) cells (1) by electro-transfection (*Capn3*$^{C129S\text{-}neo}$). Among the 120 ES colonies that survived in G418 selection medium, 6 were positive for the targeting vector as determined by PCR screening (see B). The recombinant ES cell lines were also characterized by Southern blot analysis (see C). Isolated genomic DNA was digested with *Afl*II or *Stu*I+*Bam*HI, and hybridized with the 5' or 3' probe indicated. Cell lines #32 and #55 were used for blastocyst injection, and both produced germline-transmitted chimeric mice. The F1 heterozygotes (*Capn3*$^{C129S\text{-}neo/+}$) were analyzed by Southern blot analysis (see D) to confirm proper recombination, and were crossed with transgenic mice expressing the Cre recombinase in germline cells, B6.FVB-TgN(EIIa-Cre)C5379Lmgd (2). Both the #32 and #55 lines produced mice with the C129S mutation without *neoR* (*Capn3*^{C129S}), which was confirmed by PCR and Southern blot analyses (see D), and eventually showed apparently identical phenotypes (data not shown). Therefore, the #55 line was used for further experiments. The p94KI mice were backcrossed with C57BL/6 J mice for more than 8 generations. The mouse genotypes were determined by genomic Southern blot and PCR analyses. The PCR primers are listed in Table S2.

The numbers indicate exons. LoxP sites were inserted on both sides of a *neoR* cassette. PCR1 and PCR2 indicate the amplified regions used to detect the allele by homologous recombination. DT-A, diphtheria toxin A fragment.

(**B**) PCR screening of ES cell colonies. Genomic DNA isolated from G418-resistant ES cell lines was subjected to PCR amplification of the targeted region shown in (A) as "PCR1". Closed and open arrowheads indicate the amplified bands of the WT and mutant samples, respectively. ht, heterozygous; HM, homozygous.

(**C**) Southern blot analysis of F1 mice. Genomic DNA isolated from the tails of mice resulting from crosses between targeted chimeras and WT mice was digested with *Afl*II or *Stu*I+*Bam*HI, and subjected to Southern blot analysis using the 5' and 3' probes indicated in A. Closed and open arrowheads indicate bands corresponding to the WT and mutant alleles, respectively. ht, heterozygous.

(**D**) Southern blot and PCR analysis of p94KI. Genomic DNA from mice derived from crosses between p94KI and WT mice was digested with *Pvu*II and subjected to Southern blot analysis using the ex.3 probe indicated in A (upper). The same genomic DNA was subjected to PCR amplification using the same conditions as in (B) (lower). Closed and open arrowheads indicate bands corresponding to the WT and mutant alleles, respectively. ht, heterozygous; HM, homozygous.

(**E**) Confirmation of the C129S mutation in p94KI mice. Genomic DNA from the mouse tail was amplified by PCR and digested by *Pvu*II, generating fragments of 662 and 108 bp (open arrowheads) for homozygotes (HM), 730 bp (closed arrowheads) for WT mice (WT), and 108, 662, 730, and 770 bp for heterozygotes (ht).

(**F**) Proteolytic inactivity of p94 in p94KI mice. Equal amounts of protein from skeletal muscle lysates of WT and p94KI mice (15-weeks old) were incubated with 10 mM EDTA or 5 mM $CaCl_2$ at 30°C for 30 min. Full-length p94 (arrow) and its proteolytic fragments (arrowheads) were detected with an anti-p94 (pIS2C) antibody. -, no treatment; E, +EDTA; C, +Ca^{2+}.

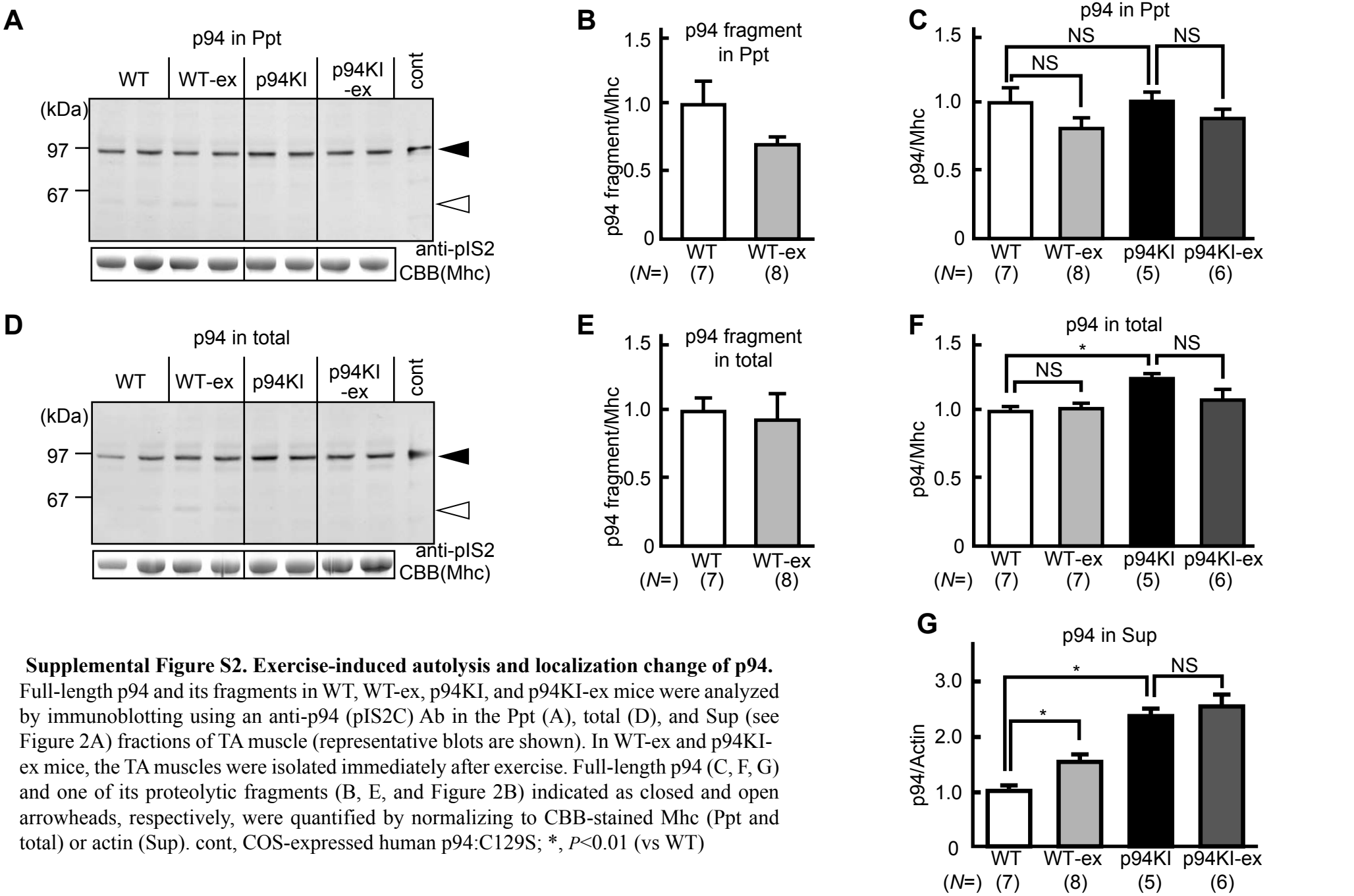

Supplemental Figure S2. Exercise-induced autolysis and localization change of p94. Full-length p94 and its fragments in WT, WT-ex, p94KI, and p94KI-ex mice were analyzed by immunoblotting using an anti-p94 (pIS2C) Ab in the Ppt (A), total (D), and Sup (see Figure 2A) fractions of TA muscle (representative blots are shown). In WT-ex and p94KI-ex mice, the TA muscles were isolated immediately after exercise. Full-length p94 (C, F, G) and one of its proteolytic fragments (B, E, and Figure 2B) indicated as closed and open arrowheads, respectively, were quantified by normalizing to CBB-stained Mhc (Ppt and total) or actin (Sup). cont, COS-expressed human p94:C129S; *, $P<0.01$ (vs WT)

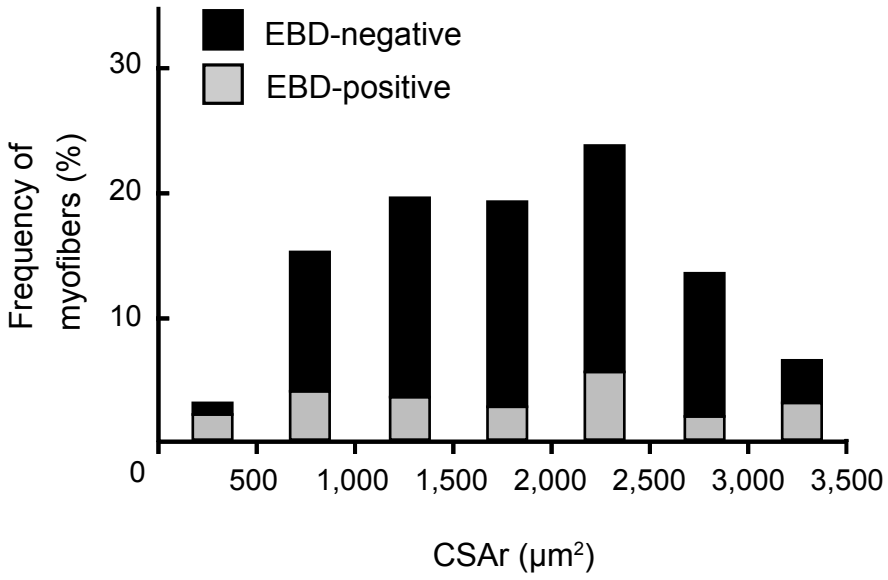

Supplemental Figure S3. Frequency distribution of EBD-negative and -positive myofiber CSArs in the Gastrocnemius (GC) of p94KI-ex mice on post-exercise day 1

A total of 378 EBD-negative (undamaged) and 110 EBD-positive fiber profiles were traced in two sections from each of three p94KI-ex mice. The average CSAr was 1,817 μm^2 and 1,933 μm^2 for the EBD-negative and -positive myofibers, respectively, showing no statistically significant difference.

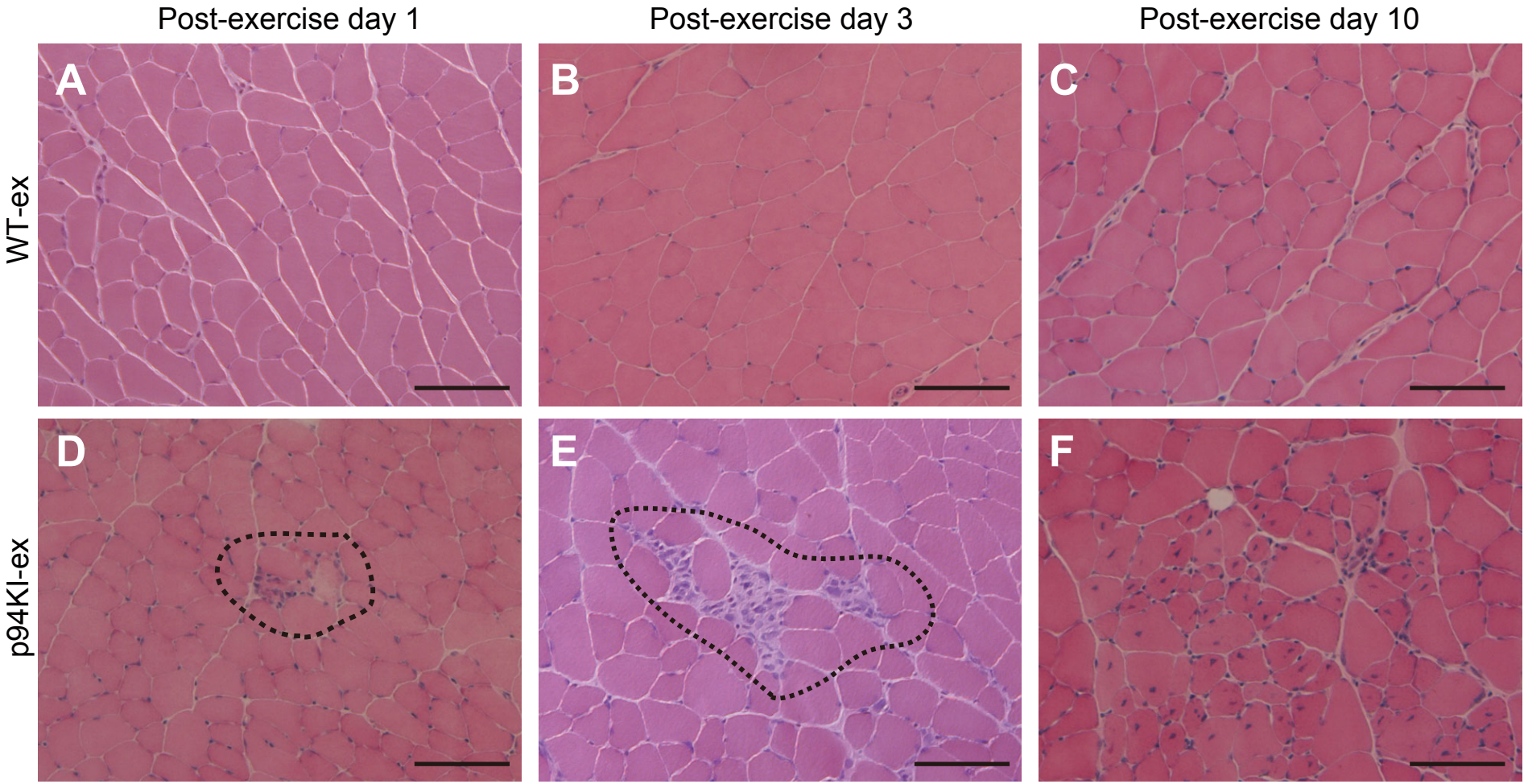

Supplemental Figure S4. Normal muscle regeneration was observed in exercised p94KI mice. Muscle regeneration processes were observed in HE-stained gastrocnemius muscles from WT-ex (A-C) and p94KI-ex (D-F) mice. Muscles were prepared on the indicated days after exercise. The invading cells and proliferating myogenic cells were observed in p94KI-ex mice (dotted areas in D and E). Small-diameter myofibers with central nuclei are de novo regenerated myofibers (F). WT-ex mice showed no obvious damage (A-C). Bars, 100 μm.

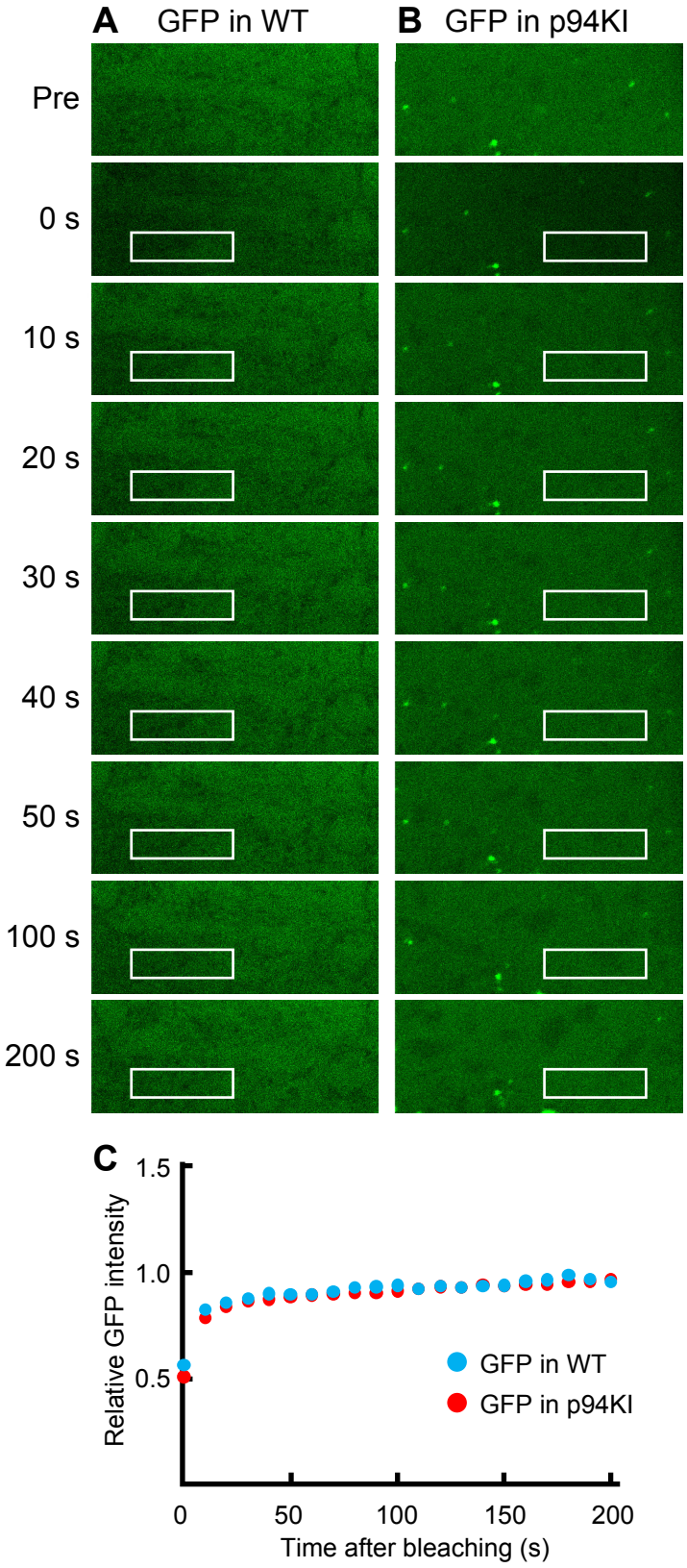

Supplemental Figure S5. Control experiments for FRAP studies of Figure 3C.
(**A and B**) FRAP observation of GFP expressed in cultured myotubes. Representative series of micrographs are shown. GFP was exogenously expressed in cultured myotubes from WT (A) or p94KI (B) mice by the transfection of pEGFP empty vector into the myotubes. GFP showed diffuse and uniform signals in the cytosol without striation. Reference images were acquired before photobleaching (Pre). Rectangles indicate the photobleached areas. (**C**) Relative fluorescence intensities in the areas were calculated by LSM software as the ratio of GFP intensity at each time point to that before photobleaching, and plotted against time. The GFP signals could not be photobleached to 0% because the mobility of GFP in the cytosol was too fast, and was quickly recovered to almost to 90% within 30 s.

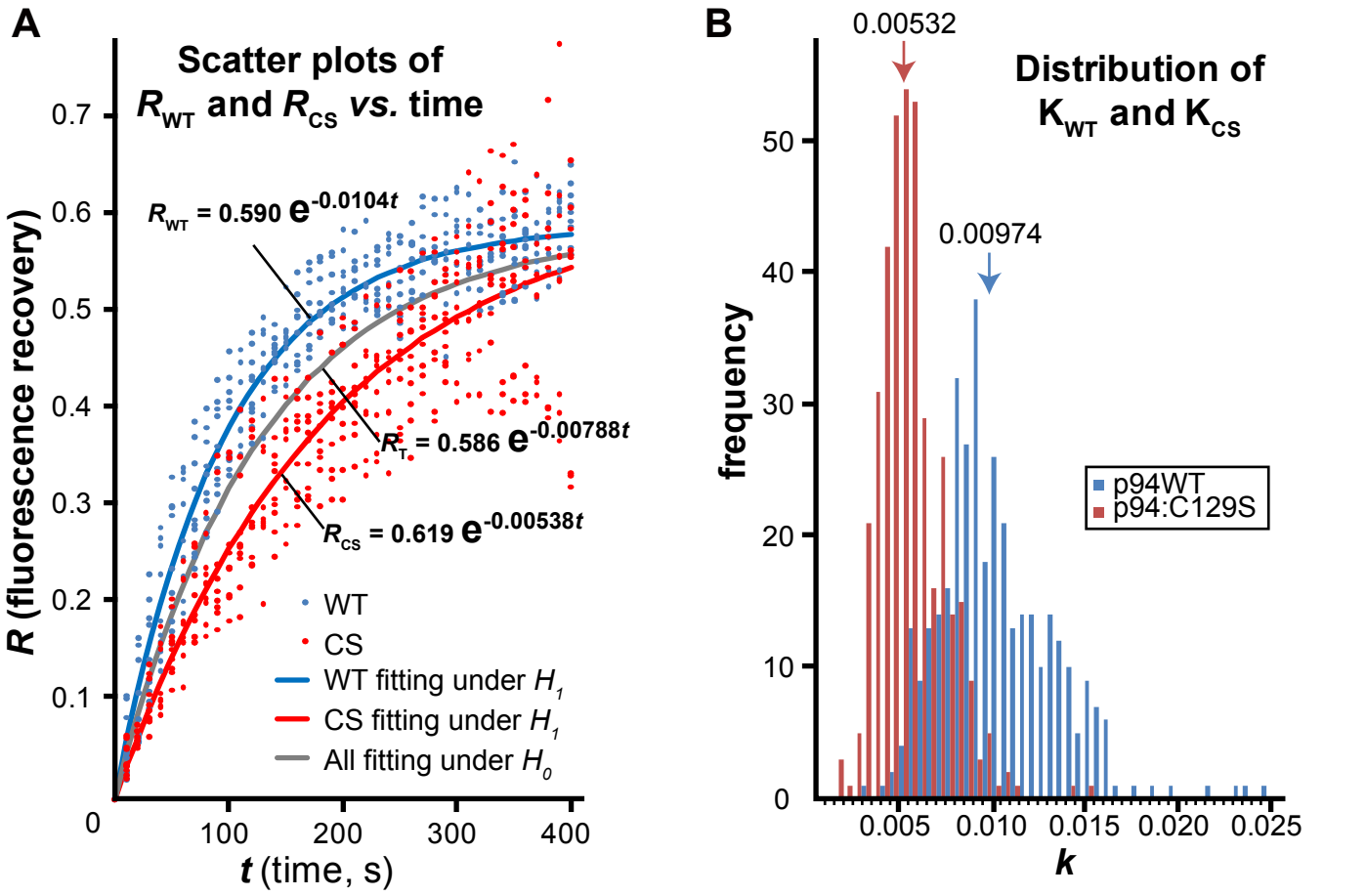

Supplemental Figure S6. Statistical tests for the significant difference between the k values for p94WT and p94:C129S in Figure 3C.

(A) Scatter plots of $\boldsymbol{R}$ *vs.* time and analysis of covariance. Observation time ($\boldsymbol{t}$, s) and relative recovery of GFP fluorescence intensity ($\boldsymbol{R}_{WT}$ and $\boldsymbol{R}_{CS}$ for p94WT (WT) and p94:C129S (CS) experiments, respectively) were well fitted to the equation, $\boldsymbol{R} = M(1 - e^{-k\boldsymbol{t}})$, and we obtained estimated values of M and k for both WT and CS (M_{WT}, k_{WT}, M_{CS}, and k_{CS} are estimated to be 0.590, 0.0104, 0.619, and 0.00538, respectively, as shown here and in Figure 3C).

First, the following two hypotheses are taken: H_0: $k_{WT} = k_{CS}$ and H_1: $k_{WT} \neq k_{CS}$ (both sides)

Under H_1, the residual sums of squares for WT and CS are calculated using each of 400 data pairs (($\boldsymbol{R}_{WTi}$, $\boldsymbol{t}_i$) and ($\boldsymbol{R}_{CSi}$, $\boldsymbol{t}_i$) [i = 1 to 400]):

$$\Delta\text{WT} = \sum_{i=1}^{400}\left(\boldsymbol{R}_{WT_i} - M_{WT}(1 - e^{-k_{WT}\boldsymbol{t}_i})\right)^2 = 0.562;\ \Delta\text{CS} = \sum_{i=1}^{400}\left(\boldsymbol{R}_{CS_i} - M_{CS}(1 - e^{-k_{CS}\boldsymbol{t}_i})\right)^2 = 1.590;\ \Delta 1 = \Delta\text{WT} + \Delta\text{CS} = 2.152$$

Under H_0, all 800 data pairs (400 WT and 400 CS) were fitted as described above, and the following equation was obtained:

$\boldsymbol{R}_T = M_T(1 - e^{-k_T\boldsymbol{t}})$, where M_T, and k_T are estimated to be 0.5859 and 0.00788 by the least squares method.

The residual sums of squares for all 800 data pairs were calculated using two of the 400 data pairs (($\boldsymbol{R}_{WTi}$, $\boldsymbol{t}_i$) and ($\boldsymbol{R}_{CSi}$, $\boldsymbol{t}_i$) [i = 1 to 400]):

$$\Delta 2 = \sum_{i=1}^{400}\left(\boldsymbol{R}_{WT_i} - M_T(1 - e^{-k_T\boldsymbol{t}_i})\right)^2 + \sum_{i=1}^{400}\left(\boldsymbol{R}_{CS_i} - M_T(1 - e^{-k_T\boldsymbol{t}_i})\right)^2 = 3.834$$

A statistical value, F is defined as follows: $F = \frac{\Delta 2 - \Delta 1}{\Delta 1/(N-4)} = (\frac{\Delta 2}{\Delta 1} - 1) \times (N - 4) = 578.7$, where N = the number of total samples (in our case, 400 + 400 - 56 (inappropriate data) = 744). By analysis of covariance, under H_0, F is known to follow the F distribution with the degrees of freedom, ν_1 =1 and ν_2 = N-4 [$F_{1, N-4}$]. Since the upper point where $F_{1, N-4}$ shows 0.001 probability ($F_{1, N-4}(\alpha = 0.001)$) is 10.91, and is less than the calculated F, and thus, H_0 is rejected with a significance level of 0.001 (P value for acceptance of H_0 is 1.48 x 10^{-96}). Therefore, it is concluded that $k_{WT} \neq k_{CS}$.

(B) Distribution of K and non-parametric tests. Using estimated M_{WT} and M_{CS}, k_{WT} and k_{CS} can be calculated for each of 400 data pairs of $\boldsymbol{R}$ and $\boldsymbol{t}$ for each of WT and CS. These two sets of k values, K_{WT} and K_{CS}, have 400 elements each, the distributions of which are shown here. Non-parametric tests for the difference between K_{WT} and K_{CS} were performed using Origin^{TM} 8 Pro software (Origin Lab Corp) and an "R" package "lawstat". For the Kolmogorov-Smirnov test and Wilcoxon-Mann-Whitney test, let H_0: median (K_{WT}) = median (K_{CS}) and H_1: median (K_{WT}) > median (K_{CS}). The Kolmogorov-Smirnov test showed a D value of 0.26 and P value of 2.5 x 10^{-12}, and the Wilcoxon-Mann-Whitney test showed a U value of 63,358 and P value of 3.5 x 10^{-7} (Origin^{TM} 8 Pro). Therefore, both tests indicated that the medians of K_{WT} and K_{CS} were significantly different with a risk rate of 0.001. For the Brunner-Munzel test, let H_0: p = 0.5 and H_1: p > 0.5, where $p = P(K_{WT} > K_{CS}) + \frac{1}{2} P(K_{WT} = K_{CS})$. This test does not assume any distribution pattern or homoscedasticity. Calculation with an "R" package "lawstat" showed a degree of freedom of 737.929, W value of 45.763, estimated p value of 0.927, and P value of less than 2.2 x 10^{-16}. Therefore, the Brunner-Munzel test also indicated that the averages of K_{WT} and K_{CS} were significantly different with a risk rate of 0.001. All of these analyses indicated that k_{WT} and k_{CS} estimated by two data sets, K_{WT} and K_{CS}, were significantly different, i.e., that WT and CS have significantly different recovery rates.

All four statistical tests described above also showed significant difference between the estimated WT and p94KI (KI) curves ($\boldsymbol{r}$=$Ae^{-k\boldsymbol{t}}$; A_{WT}=4.56, k_{WT}=1.01, A_{KI}=8.80, k_{KI}=1.18) shown in Figure 3Q (Parameters, in order, are: N=377, $F_{1, N-4}(\alpha$=0.001)=11.0, F=39.9, P=7.76 x 10^{-10}; D=0.68 (for A) and 0.54 (for k), P=6.46 x 10^{-39} and 1.69 x 10^{-24}; U=3,020 and 5,527, P=3.73 x 10^{-44} and 5.98 x 10^{-31}; df=368 and 365, W=29.6 and 17.7, p=0.915 and 0.845, P<2.2 x 10^{-16} and <2.2 x 10^{-16}).

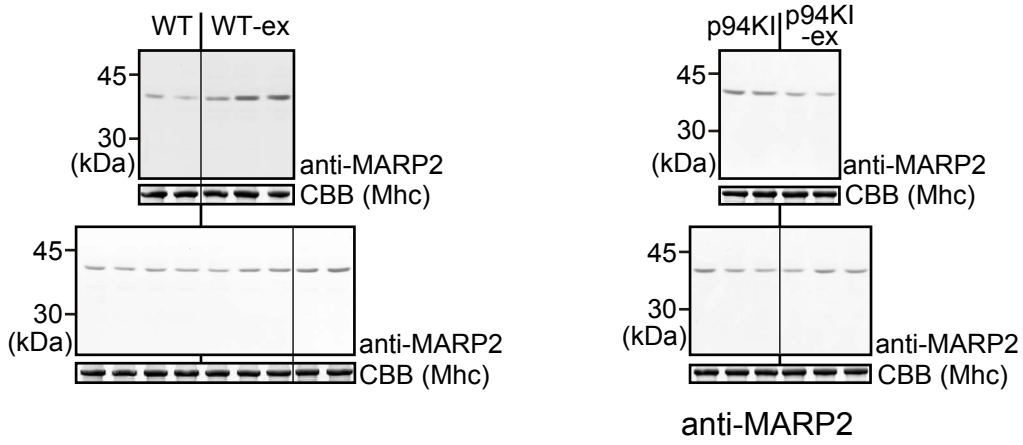

Supplemental Figure S7. Change in the MARP2 level in WT and p94KI mice after exercise.

The MAPR2 protein amounts in WT, WT-ex, p94KI, and p94KI-ex mouse muscles was analyzed by western blotting using an anti-MARP2 Ab. TA muscles (total extract) were isolated immediately after exercise. The Mhc bands stained by CBB, used as loading controls, are shown. Hairlines indicate lanes that were run on the same gel but were noncontiguous.

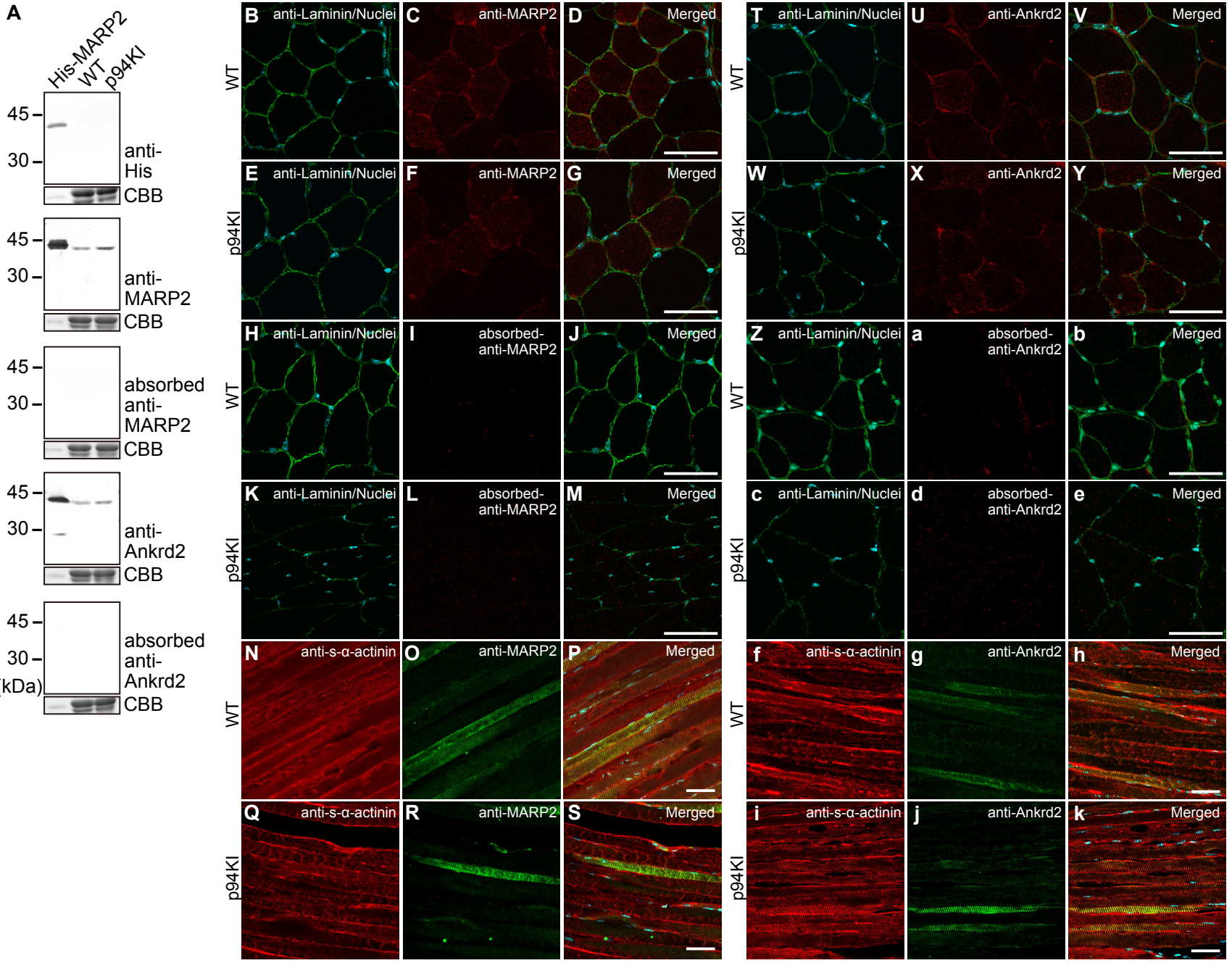

Supplemental Figure S8. Specificities of the anti-MARP2 Abs used in this study.

(A) Characterization of two anti-MARP2 Abs used in this study by immunoblot analysis. The anti-MARP2 Ab described in reference (5) and that purchased from Protein Tech Group Inc. are called "anti-MARP2" and "anti-Ankrd2" Abs for descriptive purposes here. To verify the specificity of these anti-MARP2 Abs, they were compared with those absorbed with an excess amount of recombinant His-tagged full-length human MARP2 protein (5). Sup fractions from WT (WT) and p94KI (p94KI) mouse TA muscles, and His-tagged full-length human MARP2 (His-MARP2, 50 ng/lane) as a positive control were used for immunoblot analyses with the indicated Abs. CBB-stained His-MARP2 and actin bands, used as a loading control, are shown. (B-S) Characterization of the anti-MARP2 Ab by immunostaining. Muscle cross (B-M, T-e) and longitudinal (N-S, f-k) sections from WT (B-D, H-J, N-P, T-V, Z-b, f-h), and p94KI (E-G, K-M, Q-S, W-Y, c-e, i-k) mice were stained with anti-laminin α2 (B, E, H, K, T, W, Z, c), anti-MARP2 (C, F, O, R), absorbed anti-MARP2 (I, L), anti-Ankrd2 (U, X, g, j), absorbed anti-Ankrd2 (a, d), and anti-sarcomeric α-actinin (N, Q, f, i) Abs.

Nuclei were visualized with DAPI (light blue in B, D, E, G, H, J, K, M, P, S, T, V, W, Y, Z, b, c, e, h, k). Merged images are shown in D, G, J, M, P, S, V, Y, b, e, h, and k. Bars, 50 μm.

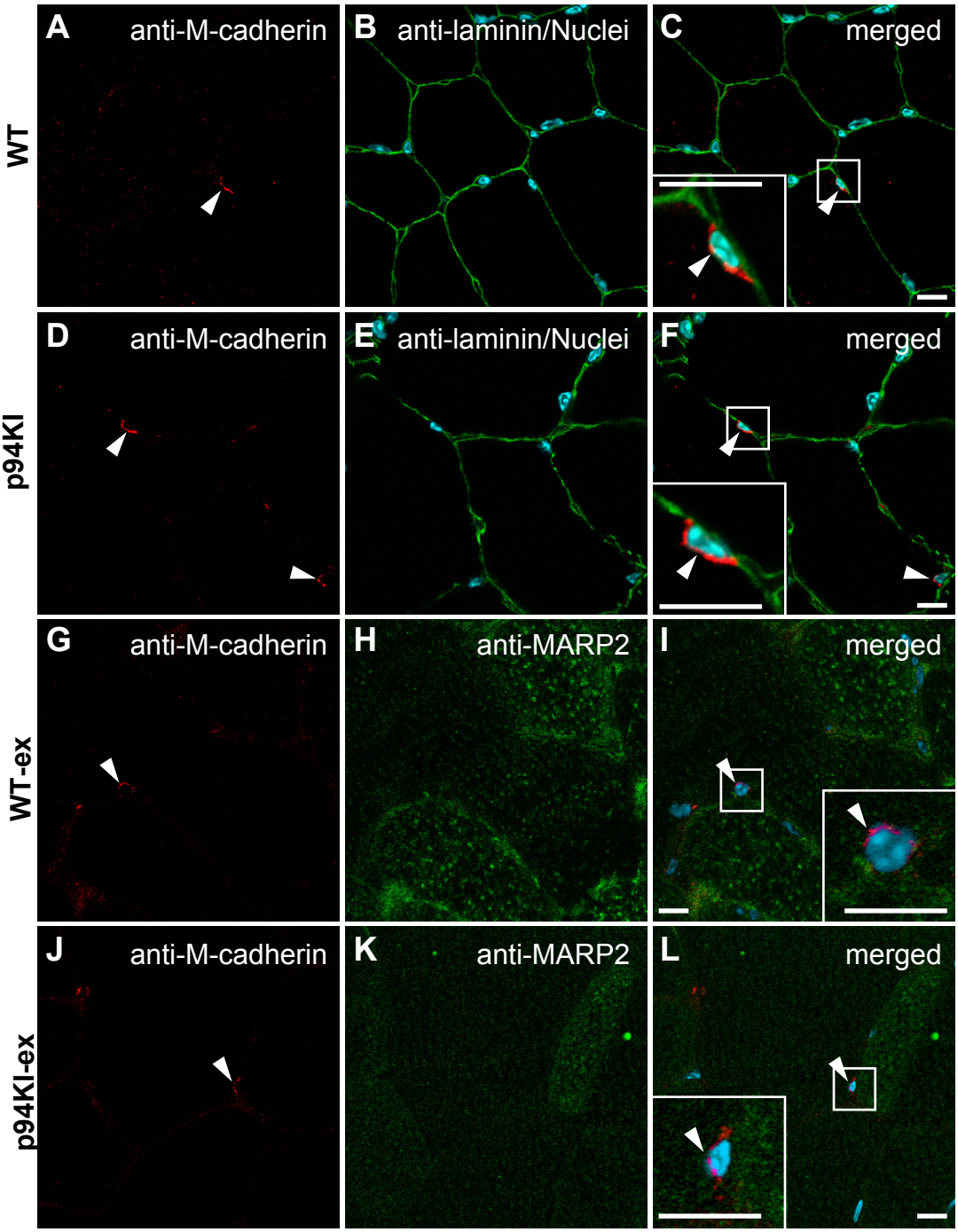

Supplemental Figure S9. MARP2 is expressed in the cytosol and in myonuclei, but not in the nuclei of satellite cells.

(**A-F**) To determine the localization of satellite cells, cryostat sections of TA muscles of WT (A-C) and p94KI (D-F) mice were immunostained with anti-M-cadherin (A and D) and anti-laminin α2 (B and E) Abs after blocking with MOM™ mouse Ig blocking reagent (Vector Laboratories, Inc.). Images were visualized by confocal fluorescence microscopy (LSM510, Zeiss). M-cadherin is a marker for satellite cells, which were located beneath the laminin-positive basement membrane (arrowheads in A, C, D, and F). (**G-L**) Confocal micrographs of M-cadherin (G and J) and MARP2 (H and K) in muscles from WT-ex (G-I) and p94KI (J-L) mice. The nuclei of satellite cells had no MARP2 signals (arrowheads in G-L).
Merged images are shown at the right (C, F, I, and L). Insets in C, F, I, and L are magnified images of the regions marked by squares. Bars, 10 μm.

Ojima et al Supplemental Figure S10

gi No.	Protein name	Gene	%Cov	p94KI /WT	*P* -value	WT-ex /WT	*P* -value	p94KI-ex /p94KI	*P* -value	DNA micro-array
13507646	heat shock protein 8	***Hspb8***	12.2	**3.60**	-	**1.59**	-	**0.79**	-	-
40644653	kinesin family member 15	***Kif15***	1.3	**2.87**	1.2E-02	**2.53**	4.5E-03	**1.07**	3.1E-01	-
29294760	ribosomal protein S6 kinase α-1	***Rps6ka1***	2.6	**2.06**	9.0E-02	**1.81**	4.5E-02	**1.70**	4.0E-01	NC
74227220	hydroxyacyl glutathione hydrolase	***Hagh***	8.1	**1.90**	-	**1.75**	-	**0.84**	-	-
149257950	28S ribosomal protein S36, mitochondrial	***Mrps36***	17.6	**1.86**	-	**1.33**	-	**1.12**	-	-
37359988	brain specific angiogenesis inhibitor 3	***Bai3***	2.0	**1.84**	2.2E-03	**1.64**	9.3E-02	**1.48**	1.7E-01	-
187957266	filamin Cγ	***Flnc***	0.9	**1.80**	4.0E-01	**1.79**	3.2E-01	**0.66**	3.2E-01	-
74220201	ubiquitin conjugating enzyme E2L3, UbcH7	***Ube2l3***	10.7	**1.71**	-	**1.70**	-	**1.24**	-	-
548879	Ras suppressor protein 1, RSP-1	***Rsu1***	6.1	**1.71**	-	**1.42**	-	**0.67**	-	NC
7305143	hexokinase 2	***Hk2***	0.9	**1.70**	1.7E-01	**1.47**	7.2E-02	**1.09**	5.2E-01	NC
76779273	chaperonin, HSP60, HSPD1	***Hspd1***	2.7	**1.64**	-	**1.65**	-	**1.06**	-	NC
51890211	leucine rich repeat containing 8 family, member E	***Lrrc8e***	1.3	**1.55**	2.3E-01	**1.60**	6.4E-02	**0.81**	6.2E-01	-
6678682	galectin 1, lectin, galactose binding, soluble 1	***Lgals1***	14.8	**1.55**	-	**1.02**	-	**1.06**	-	-
18044689	Ser (or Cys) peptidase inhibitor, clade A, member 3K	***Serpina3k***	3.6	**1.52**	9.4E-02	**1.19**	1.4E-01	**0.91**	4.0E-02	-
29244166	SH3 and cysteine rich domain 3	***Stac3***	6.4	**1.48**	-	**1.55**	-	**1.14**	-	-
74151744	proteasome subunit, alpha 4	***Psma4***	4.2	**1.45**	2.9E-01	**1.72**	1.8E-01	**1.05**	7.9E-01	-
313103	myomesin 1	***Myom1***	1.6	**1.44**	-	**1.59**	-	**1.31**	-	NC
74147026	heat shock protein 90kDa α, class B member 1	***Hsp90ab1***	15.2	**1.42**	7.3E-03	**1.44**	1.7E-03	**0.92**	2.1E-01	NC
28302235	Pif1, 5'-to-3' DNA helicase homolog	***Pif1***	2.3	**1.42**	-	**1.40**	-	**1.16**	-	-
74186554	Nedd8	***Nedd8***	25.0	**1.42**	-	**1.39**	-	**1.20**	-	-
82795783	eukaryotic translation elongation factor 1γ, eEF-1γ	***Eef1g***	2.6	**1.39**	6.3E-01	**1.40**	5.3E-01	**0.87**	8.8E-02	-
148685426	Tu translation elongation factor, mitochondrial	***Tufm***	8.3	**1.39**	8.1E-02	**1.38**	5.1E-02	**1.07**	7.1E-01	NC
158937312	heat shock protein 1	***Hspb1***	48.8	**1.37**	2.6E-02	**1.30**	1.2E-02	**0.72**	3.8E-03	-
74177941	Hsc70 interacting protein, suppression of tumorigenicity 13	***St13***	3.2	**1.36**	6.9E-02	**1.28**	4.9E-02	**0.86**	1.4E-01	-
2950347	myomesin 2, M-protein	***Myom2***	6.7	**1.36**	9.1E-04	**1.17**	6.9E-02	**1.11**	3.7E-01	-
12833697	tropomyosin 2	***Tpm2***	64.1	**1.32**	1.2E-01	**1.10**	2.2E-01	**0.95**	7.0E-01	NC
8392959	UDP-Gal:βGlcNAc β-1,4- galactosyltransferase, polypeptide 2	***B4galt2***	2.4	**1.31**	-	**1.16**	-	**0.87**	-	NC
21304450	immunoglobulin gamma1 heavy chain	***Ighg1***	5.0	**1.31**	2.2E-01	**2.66**	6.8E-02	**0.97**	8.6E-01	-
74187552	14-3-3ζ	***Ywhaz***	5.7	**1.30**	-	**1.11**	-	**1.14**	-	NC
31542970	cardiovascular heat shock protein	***Hspb7***	7.7	**1.30**	8.0E-02	**1.59**	1.9E-02	**0.76**	3.8E-02	-
74198008	glucosamine (N-acetyl)-6-sulfatase	***Gns***	1.3	**1.30**	-	**1.11**	-	**0.96**	-	-
6753530	crystallin, αB	***Cryab***	48.6	**1.29**	6.8E-03	**1.33**	1.1E-03	**0.76**	6.0E-04	NC
6753912	ferritin heavy chain 1	***Fth1***	8.2	**1.29**	-	**1.61**	-	**1.13**	-	NC
74223108	dihydrolipoamide dehydrogenase, pyruvate dehydrogenase component E3	***Dld***	13.6	**1.29**	1.8E-02	**1.36**	3.1E-02	**1.10**	1.4E-01	NC
74224118	radixin isoform a	***Rdx***	6.8	**1.28**	2.1E-01	**1.28**	1.7E-01	**1.07**	4.6E-01	NC
74184730	latrophilin 1	***Lphn1***	0.6	**1.28**	-	**1.09**	-	**1.00**	-	-
59958370	heat shock protein, α-crystallin-related, B6	***Hspb6***	14.2	**1.27**	4.2E-02	**1.23**	1.5E-02	**0.91**	8.1E-02	-
148685498	aldolase A, fructose-bisphosphate	***Aldoa***	81.3	**1.24**	1.4E-03	**1.11**	3.3E-02	**0.90**	1.4E-02	NC
6754724	proteasome 26S subunit, non-ATPase, 7	***Psmd7***	6.2	**1.24**	7.9E-01	**1.55**	2.1E-01	**0.85**	7.6E-01	-
26348052	nucleolar protein 3 (apoptosis repressor with CARD domain)	***NOL3***	8.6	**1.23**	7.0E-01	**0.94**	9.1E-01	**0.87**	6.8E-01	-
148704795	cofilin 2, muscle	***Cfl2***	64.0	**1.23**	3.8E-02	**1.14**	1.3E-01	**1.06**	1.8E-01	NC
6678391	troponin I, skeletal, fast 2	***Tnni2***	55.5	**1.22**	1.4E-01	**0.98**	7.8E-01	**0.83**	3.0E-04	NC
74147564	nicotinamide phosphoribosyltransferase	***Nampt***	1.6	**1.21**	5.1E-01	**1.05**	7.8E-01	**0.82**	3.5E-02	-
2340058	troponin T	***Tnnt3***	29.2	**1.20**	2.8E-03	**1.09**	4.7E-02	**0.90**	3.0E-03	NC
49864	α-actin	***Acta1***	67.3	**1.20**	2.3E-04	**0.98**	6.1E-01	**1.03**	3.9E-01	NC
9910130	ankyrin repeat domain 2, ANKRD2, MARP2	***Ankrd2***	4.57	**1.18**	-	**1.15**	-	**0.73**	-	-
70778976	phosphoglycerate kinase 1	***Pgk1***	78.2	**1.16**	1.3E-03	**1.06**	5.7E-02	**1.01**	8.7E-01	NC
109081395	tropomyosin 1 α chain	***Tpm1***	80.3	**1.14**	6.9E-03	**1.05**	4.3E-01	**0.92**	2.3E-01	NC
124249109	AT rich interactive domain 1A	***Arid1a***	0.7	**1.12**	4.5E-02	**1.16**	1.1E-01	**1.12**	3.9E-01	-
156257677	β-globin	***Hbb-b1***	44.9	**1.12**	1.9E-02	**0.97**	2.9E-01	**0.89**	1.2E-07	0.45
31982861	carbonic anhydrase 3	***Car3***	59.2	**0.90**	1.1E-02	**1.01**	7.4E-01	**1.26**	1.7E-16	-
148675904	malate dehydrogenase 1, NAD (soluble)	***Mdh1***	36.9	**0.89**	3.5E-02	**0.93**	1.1E-01	**1.00**	8.9E-01	NC
29789016	fast skeletal myosin alkali light chain 1 isoform 1f	***Myl1***	49.5	**0.89**	7.8E-03	**0.80**	9.0E-05	**0.82**	4.0E-05	NC
74205957	glycerol-3-phosphate dehydrogenase 1	***Gpd1***	25.8	**0.89**	3.8E-02	**0.92**	1.8E-01	**1.05**	2.3E-01	NC
10092608	glutathione S-transferase, π1	***Gstp1***	31.4	**0.87**	7.6E-03	**1.00**	9.6E-01	**1.14**	9.2E-02	NC
74150922	fumarase, fumarate hydratase, mitochondrial	***Fh1***	10.5	**0.83**	3.4E-01	**0.87**	3.3E-01	**0.97**	5.5E-01	-
6753290	calsequestrin 1	***Casq1***	14.0	**0.83**	3.4E-04	**0.90**	1.4E-02	**1.28**	1.2E-07	0.85
59798456	uncharacterized protein KIAA0256	***3110001I20Rik***	0.8	**0.83**	-	**0.88**	-	**1.17**	-	-
148679891	peroxiredoxin 1	***Prdx1***	19.6	**0.83**	3.5E-02	**1.14**	9.2E-02	**0.97**	3.8E-01	NC
74212250	lactate dehydrogenase A	***Ldha***	53.0	**0.83**	6.9E-05	**1.09**	8.6E-01	**1.02**	2.7E-01	NC
7949078	myosin regulatory light chain 2, fast skeletal muscle	***Mylpf***	13.6	**0.82**	2.5E-02	**0.82**	7.3E-02	**0.97**	7.0E-01	NC
27659728	aldo-keto reductase family 7, member A5	***Akr7a5***	8.4	**0.81**	2.1E-01	**0.94**	7.7E-01	**1.09**	5.2E-01	-
74137565	albumin	***Alb***	55.8	**0.81**	3.7E-16	**1.05**	2.3E-02	**1.05**	5.8E-04	NC
148669989	glutathione S-transferase M1	***Gstm1***	13.7	**0.81**	3.9E-02	**0.92**	3.7E-01	**0.94**	4.4E-01	-
31982522	acyl-Coenzyme A dehydrogenase, short chain	***Acads***	8.3	**0.80**	1.6E-02	**0.83**	1.7E-01	**1.01**	3.9E-01	-
9963904	profilin 2	***Pfn2***	17.9	**0.77**	2.8E-02	**0.89**	1.8E-01	**1.11**	1.6E-01	-
6679937	glyceraldehyde-3-phosphate dehydrogenase	***Gapdh***	71.8	**0.76**	1.9E-17	**1.06**	8.2E-01	**0.98**	1.5E-01	NC
74144566	DnaJ (Hsp40) homolog, subfamily B, member 14 isoform 8	***Dnajb14***	5.1	**0.74**	2.8E-07	**0.77**	9.4E-08	**1.01**	6.2E-02	-
146345417	electron transfer flavoprotein subunit α, mitochondrial; α-ETF	***Etfa***	20.7	**0.74**	4.0E-03	**0.89**	2.3E-01	**1.01**	8.8E-01	-
6680690	peroxiredoxin 3	***Prdx3***	5.4	**0.73**	-	**0.88**	-	**0.98**	-	-
84794552	phosphatidylethanolamine binding protein 1, Raf kinase inhibitor protein	***Pebp1***	46.5	**0.70**	6.7E-03	**0.82**	1.2E-02	**1.00**	9.6E-01	NC
31980767	parvalbumin	***Pvalb***	88.2	**0.69**	3.6E-12	**0.79**	3.5E-07	**0.99**	7.0E-01	NC
21359820	myoglobin	***Mb***	85.7	**0.64**	2.6E-27	**0.78**	9.3E-19	**0.92**	4.7E-03	NC
13385680	2,4-dienoyl CoA reductase 1, mitochondrial	***Decr1***	4.5	**0.59**	9.6E-02	**0.66**	6.8E-02	**0.92**	1.1E-02	-
50510361	peroxiredoxin 6	***Prdx6***	8.4	**0.40**	-	**0.59**	-	**1.22**	-	NC

Supplemental Figure S10. Proteins with significantly different expression in the cytosol of WT and p94KI skeletal muscles.

Relative protein expression amounts of WT, WT-ex, p94KI, and p94KI-ex mice were analyzed by iTRAQ^{TM}-labeling, 2D-LC-MALDI-TOF/TOF, and ProteinPilot^{TM} software. Proteins that have %Cov of non zero value and show p94KI/WT of WT/p94KI>1.1 are listed here in order of the p94KI/WT value (%Cov means % of amino acid residues (aar) included in the identified peptides with a confidence level of more than 95 against total aar of the protein). Ratios of greater than 1.1, greater than 1.2, less than 1/1.1 (0.91), and less than 1/1.2 (0.83) are marked by red, orange, pale blue, and blue colors, respectively. *P*-values were calculated by the ProteinPilot^{TM} program for proteins that are identified by more than one peptide; otherwise, they are shown by "-". *P*-values less than 0.05 are colored yellow. For proteins that had no *P*-value due to single MS/MS identification or a *P*-value of more than 0.05, MS/MS spectra were manually examined and verified, and are listed only if the MS/MS spectra were clear enough to represent a change in ratios. mRNA expression profiles are shown for genes on the DNA microarray (see Supplemental Table S1); NC, not significantly changed; -, not included in the microarray chip used.

Note that hexokinase 2, one of the rate-limiting enzymes for glycolysis, and factors involved in protein translation (EF-Tu and eEF-1γ), and proteasome subunits (PSMA4 and PSMD7) were upregulated in p94KI and WT-ex compared with WT (category **b** in Table 1). Members of this group may contribute to turnover of muscle cells by providing ATP, and producing and destructing proteins. Also, UbcH7, Nedd8, RSK-1 and S36mt, which are involved in protein degradation and translation systems, are also upregulated in WT-ex and p94KI (compared with WT) and p94KI-ex (compared with p94KI) (category **a** in Table 1). On the other hand, calsequestrin 1 (CASQ1), parvalbumin and myosin regulatory light chain 2, which binds Ca^{2+}, are all downregulated in p94KI and WT-ex compared with WT (category **d** in Table 1).

Troponin I2 (TNNI2) and nicotinamide phosphoribosyltransferase (NAMPT) were upregulated in p94KI (compared with WT), but downregulated in p94KI-ex (compared with p94KI), whereas WT-ex showed no difference from WT. Conversely, programmed cell death protein 11 (PDCD11 or ALG-4) and carbonic anhydrase 3 (CAR3) were downregulated in p94KI (compared with WT), but upregulated in p94KI-ex (compared with p94KI), whereas WT-ex showed no difference from WT. These proteins may correspond to those perturbed upon exercise without p94 protease activity, but are modulated to be unchanged during exercise in WT mice.